12th International Renewable Energy Storage Conference, IRES 2018

Passive Hybrid Storage Systems: Influence of circuit and system design on performance and lifetime

Thorsten Grün*[,a], Anna Smith[b], Helmut Ehrenberg[b], Martin Doppelbauer[a]

[a]*Karlsruhe Institute of Technology (KIT), Institute of Electrical Engineering (ETI), Hermann-von-Helmholtz-Platz 1, 76344 Eggenstein-Leopoldshafen, Germany*
[b]*Karlsruhe Institute of Technology (KIT), Institute for Applied Materials (IAM), Hermann-von-Helmholtz-Platz 1, 76344 Eggenstein-Leopoldshafen, Germany*

Abstract

Depending on the nature of a particular energy storage technology, an equivalent storage system will lead to a characteristic performance. In an extreme case the system will either provide high power (if based on capacitors) or high energy (if based on lithium ion batteries). On the other hand it will lack in energy or power, respectively. Therefore, a passive parallel connection of unlike energy storage technologies is very attractive to improve cycle life as well as power and energy density in comparison to single energy storage technologies. In this approach, different lithium ion technologies are connected with different supercapacitor technologies directly in parallel. Experimental and model-based investigations show, how the energy and power density characteristics of such systems differ from each other and which advantages can be achieved in comparison to commercial systems.

1. Introduction

The improvement of energy storage systems is gaining importance as our power demands for mobile and

———————

* Corresponding author. Tel.: +49-721-608-28282; fax: +49-721-608-28284.
  E-mail address: thorsten.gruen@kit.edu

stationary energy supplies increase. Modern energy storage technologies will deliver either high power or high energy densities. Obviously, other aspects like cycle life, costs, weight and safety have to be considered also when choosing one technology over another. For instance, lithium ion batteries (LIBs), which have a great storage capacity, will experience multiple ageing effects due to prolonged cycling or high currents dis/charge (C-rates) [1]. High lifetimes can only be achieved, if their storage system is oversized. Thereby, the depth of dis/charge and peak currents for individual cells will be reduced. On the Other hand, supercapacitors (SCs) have a very high cycle life and are able to supply high peak currents but are clearly lacking in the ability to store greater amounts of energy. The latest developments in the SC technology are hybrid capacitors, or more specific lithium ion capacitors (LICs). They are bridging the gap between LIBs and SCs as an internal hybrid system with higher energy density than SC due to their high voltage limits (between 2.2 and 3.8 V) and better cycle life and power density than LIBs [2]–[4].

Load profiles for new fields like electric applications (e.g. electric and hybrid electric vehicles or the intralogistics sector) are comprised of relatively high peak-to-average loads which arise from rapid accelerations and regenerative braking. This demand of high cycle numbers with high C-rates can't be fulfilled by a single energy storage system (ESS). However, a hybrid energy storage system (HESS), which combines at least two storage technologies, is able to meet those challenges.

For the hybridization of ESSs several approaches exist. In a review [5] three approaches where shown in which ways a HESS can be designed. First of all a HESS can be designed as a Passive Hybrid Energy Storage System (PHESS) in which SC and LIB technologies are connected directly with each other. Especially in terms of a parallel connection the system design has to consider the voltage characteristic of each technology, which means that extra LIBs or SCs have to be added in serial to match the given voltage ranges. As an example, SCs which are based on active carbon as electrode material and organic electrolytes have a voltage range of 0 to 2.7 V, whereas the voltage of commercial LIBs is typically 2.0 – 4.2 V (depending on the cathode material). Hence, the operational voltage range of a PHESS is restricted by the upper and/or lower voltage level of that component, which would be violated. To avoid any possibility of confusion we define SC as a general term to describe any supercapacitor technology including LIC and we would like to introduce the definition of an ultracapacitor (UC) which describes most of the supercapacitors consisting of active carbon electrodes.

HESSs in which at least one component is connected to power electronics, are called a semi-active hybrid energy storage system (SAHESS). In active hybrid energy storage systems (AHESSs) both storage technologies are connected to power electronics. Such systems can be found in stationary applications, like photovoltaic systems and also in the automotive sector [6], [7]. In general, HESS, which use power electronics (like SAHESS and AHESS), have some advantages over PHESS systems. Due to the active control, the energy flow within those systems is optimized and the battery lifetime can be increased more than in PHESS applications [8]. Nevertheless PHESS systems achieve a higher energy efficiency due to the fact, that no power electronic are used [9]. Such systems are also more reliable and easier to implement due to the lack of both extra power supply and additional software [10]. Power and energy density can be influenced by the sizing of the LIB and the SC unit [4] and also by the load profile [11]. For example constant load profiles will result in greater battery utilization, whereas pulsed load profiles exploit the capacitor characteristics.

In our approach, we set up a PHESS through a parallel connection of LIBs and SCs. To be more precise, we use two different LIBs and connect them directly in parallel first to a LIC and second to a UC. We show via experimental and model-based investigations how the energy and power density characteristics of such connections vary compared to sole LIBs or SCs/LICs and present a comparison to ESSs in pulsed load applications.

2. Principles and modeling of passive hybrid systems

2.1. Modeling of lithium ion batteries

For an accurate modeling of a PHESS it is mandatory to consider the electrical behavior of the system components. For our LIB model we have chosen the Thevenin model [12], which is a common method for describing LIBs [13], [14]. It consists of a voltage source $U_{ocv,battery}$, the ohmic resistance $R_{battery}$ and one RC-circuit (with R_p and C_p). Its electrical circuit model (ECM) is presented in Fig. 1.
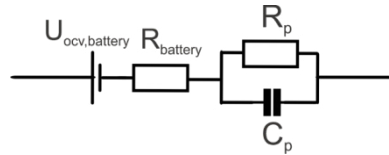
Fig. 1. ECM according to the Thevenin model of a LIB.

$R_{battery}$ represents overvoltage effects caused by the electrodes, separator and the electrolyte. It depends on the cell chemistry and the State of Charge (SOC). The RC-circuit (R_p and C_p) represents all transient cell overvoltage effects like diffusion, charge transfer and double layer effects. R_p and C_p were determined by using the Matlab Optimization Toolbox like it is described in [15]. Herein, a nonlinear Levenberg-Marquardt algorithm is used to fit the parameters R_p and C_p in the least square sense to minimize the error between the modeled LIB voltage and the measured voltage.

To obtain experimental data for the LIB components two commercially available, cylindrical LIB cells were used. One has a capacity $C_{battery}$ of 3 Ah, a format of 26650 and is based on lithium iron phosphate (LFP). The other one holds 2.45 Ah, has the 18650 format and consists of lithium cobalt oxide (LCO). $R_{battery}$ and $U_{OCV,battery}$ were measured for four LFP and LCO cells. We have chosen those two cell chemistries due to their differences in the open circuit characteristics. The measured $U_{ocv,battery}$ are depicted in Fig. 2 and it can be seen that LFP shows a very shallow slope, whereas LCO has a more continuous slope. For the measured data we would like to refer to our previous work [16].

In LIBs the value of $R_{battery}$ depends on the SOC. Therefore, we determined experimentally $R_{battery}$ at several SOCs for charge and discharge direction under the following conditions: the cell was brought to a defined SOC and paused for relaxation of the OCV, then a 0.5 C pulse of 20 s duration in either charge or discharge direction, respectively, was applied (LFP: 1.5 A; LCO: 1.2 A). Using Ohm's law, $R_{battery}$ can be calculated from the resulting change in voltage caused by the applied current. This procedure was done for a SOC window of 10 – 90 % in 10 % steps.
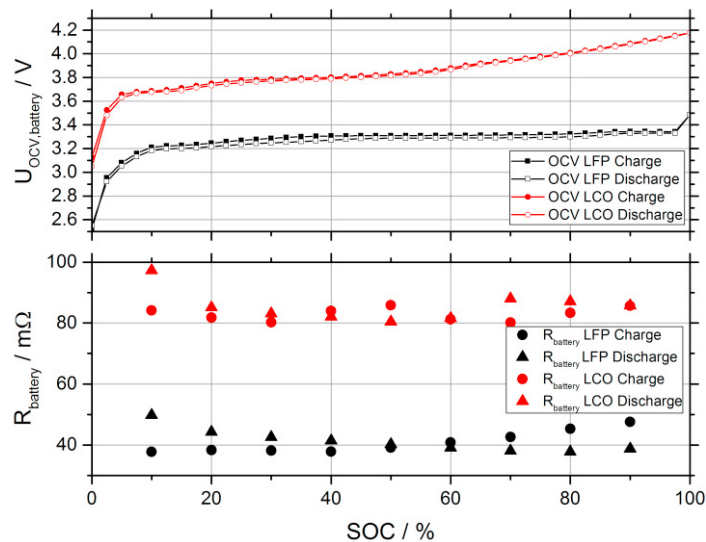

Fig. 2. Measured open circuit voltages for LFP and LCO (top). Measured internal resistance of LFP and LCO in charge and discharge direction (bottom).

2.2. Modeling of supercapacitors

The ECM of the SC is presented in Fig. 3. It consists of a voltage source $U_{ocv,cap}$ and an ohmic resistance, R_{cap}, which describes the internal resistance [17].
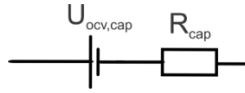
$$U_{ocv,cap} \quad R_{cap}$$

Fig. 3. ECM of a SC.

To obtain model input values for $U_{ocv,cap}$ the SCs were experimentally charged and discharged with 1 C (LIC: 1.2 A; UC: 2.25 A) within the given voltage ranges of each technology (see Table 1). Since SCs are known for their low internal resistances, in contrast to LIBs, we assume a very low influence of the internal cell resistance R_{cap} on the results and estimate this method as adequate for low currents. R_{cap} was determined for several SOCs using 1 C discharge pulses of 2 s. The results are given in Fig. 4. R_{cap} only varies by approx. 0.2 – 0.4 mΩ within the entire SOC window. Therefore, R_{cap} is considered as a constant ohmic resistance in the simulation (arithmetic mean value LIC: 1.3 mΩ; UC: 0.16 mΩ).
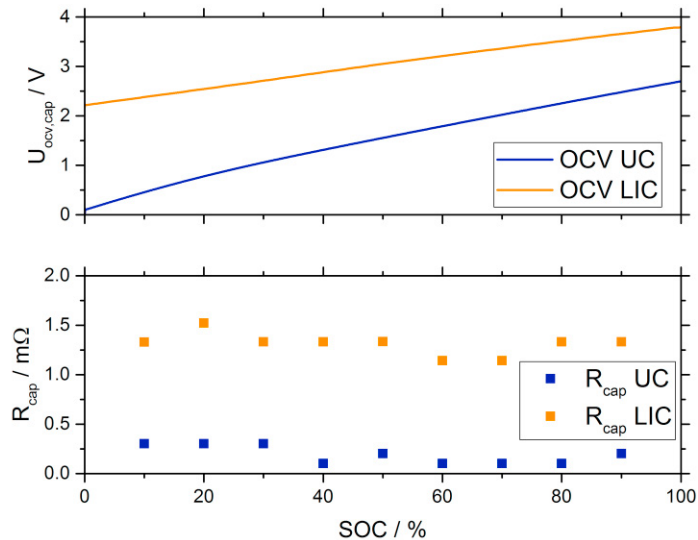
Fig. 4. Measured voltage characteristic for SC technologies (top). Measured internal cell resistance for SC technologies (bottom).

2.3. Battery and capacitor bank system model

In applications, like 48 V ESSs, several LIBs are connected in a serial and parallel manner (considered as a bank) to power the application. An application-oriented PHESS consists of a LIB and a SC bank. Herein, the amount of serial ($s_{battery}$) and parallel ($p_{battery}$) connected cells within the LIB bank and the amount of serial (s_{cap}) and parallel (p_{cap}) connected cells within the SC bank has to be defined (see Fig. 5). The kind and amount of serial and parallel connections influences the resistance of the system. In a serial connection the total resistance increases with the number of cells. In a parallel connection the total resistance decreases with the number of cells.
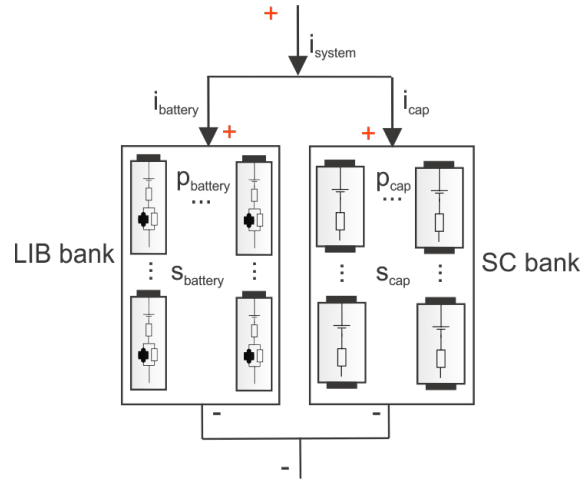
Fig. 5. Schematic representation of a PHESS divided into LIB and SC bank with respect to serial and parallel connected cells.

For the simulation of those systems the total resistance of the LIB bank $R_{battery,bank}$ and the SC bank $R_{cap,bank}$ are expressed using Eq. 1 and Eq. 2. Additional resistances of the connectors are not considered.

$$R_{battery,bank} = \frac{s_{battery}}{p_{battery}} R_{battery} \tag{1}$$

$$R_{cap,bank} = \frac{s_{cap}}{p_{cap}} R_{cap} \tag{2}$$

The serial connection of cells increases the voltage of the bank, whereas the parallel connection increases the capacity. To adapt the voltages as well as the capacities of the single cells to a bank system the following Eq. 3 – 7 hold:

$$U_{ocv,battery,bank} = U_{ocv,battery} s_{battery} \tag{3}$$

$$U_{RC,battery,bank} = U_{RC,battery} s_{battery} \tag{4}$$

$$U_{ocv,cap,bank} = U_{ocv,cap} s_{cap} \tag{5}$$

$$C_{battery,bank} = C_{battery} p_{battery} \tag{6}$$

$$C_{cap,bank} = C_{cap} p_{cap} \tag{7}$$

Table 1. Overview of cell characteristics based on different technologies

Cell type	Capacity / Ah	Resistance / mΩ	Voltage range / V	Mass / kg	Volume / l
LCO 18650	2.45	80.4 – 97.2	2.5 – 4.2	0.045	0.017
LFP 26650	3.00	38.1 – 49.8	2.0 – 3.6	0.085	0.036
LIC pouch	1.20	1.1 – 1.5	2.2 – 3.8	0.250	0.150
UC cylindrical	2.25	0.1 – 0.3	0 – 2.7	0.540	0.390

To describe the setup of PHESS in terms of parallel and serial connected cells with respect to LIBs and SCs within the system the following declination is used:

$s_{battery}$	**S**	$p_{battery}$	**P**	‖	p_{cap}	**S**	p_{cap}	**P**
Number of serial LIBs		Number of parallel LIBs			Number of serial SCs		Number of parallel SCs	

The following examples will show how our PHESS is described in terms of the circuit (number of parallel and serial connection) and system setup (which technologies are used):

- LFP$_{LIC}$ 1S1P‖1S1P → 1 LFP connected in parallel with 1 LIC
- LCO$_{UC}$ 1S1P‖2S1P → 1 LCO connected in parallel with 2 serial connected UC

3. Mathematical method

The calculation of the current distribution is based on Kirchhoff's current (KCL) and Kirchhoff's voltage law (KVL), which describe the voltage and current behavior within electric circuits. Adapted to the ECM of Fig. 5, the current distribution can be expressed as a dynamic linear optimization problem with constraints in matrix format.

The vector $\vec{\imath}$ represents the current for each node. Matrix $\underline{R}(t)$ contains the ohmic resistances of the network for each current path. It is represented as time dependent, reasoned by the dependency of $R_{battery}$ on the SOC. The vector $\vec{u}(t)$ includes $U_{ocv,battery}$ and $U_{ocv,cap}$ as well as the over-voltages due to the RC-circuit U_{RC}. Last, it contains the total current of the system i_{system} and the LIB current $i_{battery}$. In our problem, the matrix $\underline{R}(t)$ is a square matrix (n x n), where it is possible to calculate the solution by using Cramer's rule. The difference between i_{system} and $i_{battery}$ leads to the current of the SC i_{cap}. Eq. 8 presents the linear optimization problem with respect to the design of the LIB and SC bank.

$$\underline{R}(t)\vec{\imath} = \vec{u}(t)$$

$$\begin{bmatrix} 1 & 0 \\ \left(-R_{cap}\dfrac{s_{cap}}{p_{cap}}\right) & \left[\left(R_{cap}\dfrac{s_{cap}}{p_{cap}}\right) + \left(R_{battery}\dfrac{s_{battery}}{p_{battery}}\right)\right] \end{bmatrix} \begin{pmatrix} i_{system} \\ i_{battery} \end{pmatrix}$$
$$= \begin{pmatrix} i_{system} \\ \left(U_{ocv,battery} + U_{RC,battery}\right)s_{battery} - U_{ocv,cap}s_{cap} \end{pmatrix} \tag{8}$$

The current through the SC bank i_{cap} results from the difference of $i_{battery}$ and i_{system} given in Eq. 9.

$$i_{cap} = i_{system} - i_{battery} \tag{9}$$

4. Analysis

4.1. Experimental setup

In the experimental part of our investigation we determine the energy and power density of the chosen cells, as well as of the following four PHESS setups:

- LFP_{LIC} 1S1P‖1S1P
- LCO_{LIC} 1S1P‖1S1P
- LFP_{UC} 1S1P‖2S1P
- LCO_{UC} 1S1P‖2S1P

For the characterization we have chosen a proposal from the literature [18] with the following testing procedure: First, the PHESS is charged until the upper cut-off voltage is reached. Thereafter, discharge pulses of 10 s duration are applied until the lower cut-off voltage is reached. This procedure is repeated for several different current load pulses of the same duration in discharge direction. The pulse time of 10 s is chosen based on the specifications of maximum allowed current duration for 48 V power storage systems used in intralogistics. For the single LIC we have chosen the maximum current, which is allowed according to the datasheet (for UC it is approx. 1000 A but due to the restriction of our used Basytec HPS tester only a max. current of 200 A was possible). This restriction should be kept in mind for interpretation of the results.

The LIBs are discharged with a max. of 1 C, which is for our assumption the maximum allowed current. An overview of the voltage and current ranges for the experimental setup is presented in Table 2.

Table 2. Voltage limits of the different technologies and current ranges tested.

Cell type	LIC	UC	LFP	LCO	PHESS LFP_{LIC}	PHESS LCO_{LIC}	PHESS LFP_{UC}	PHESS LCO_{UC}
Voltage range/ V	2.2 – 3.8	0 – 2.7	2.0 – 3.6	2.5 – 4.2	2.2 – 3.6	2.5 – 3.8	2.0 – 3.6	2.5 – 4.2
Current range/ C	28 – 115	22 – 88	0.25 – 1	0.25 – 1	0.25 – 3	0.25 – 3	0.25 – 3	0.25 – 3

Basytec HPS battery tester was used, which measured i_{system} and the voltage of the SC U_{cap}. The current of the LIB was determined based on the measured voltage drop of a shunt resistance (0.1 mΩ) and calculated via Ohm's law. An Agilent Keysight 3872A data logger measured the voltage of the LIB $U_{battery}$. A schematic of the test bench can be seen in Fig. 6.
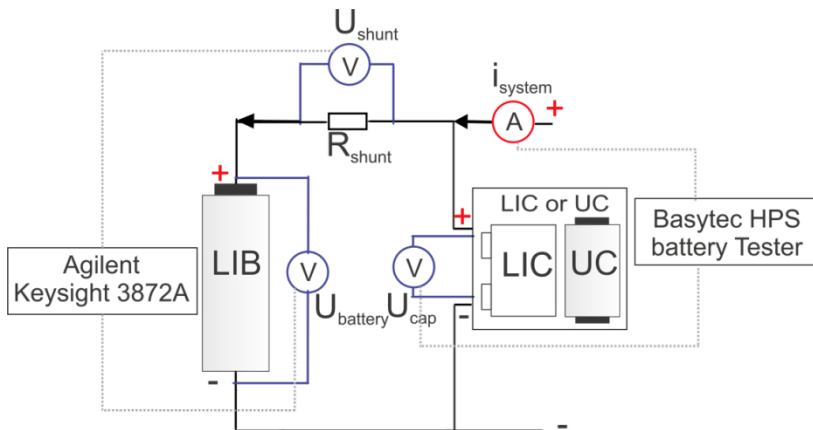

Fig. 6. Experimental setup for the characterization of PHESS.

4.2. Evaluation method for specific power and specific energy

The specific energy is calculated by integrating the product of voltage and current of each part of the PHESS over the total test time τ. The factor g(t) is used to consider only the sequences in which the discharge pulse is active (g(t)=1). In the pauses the factor g(t) is set to zero (see Fig. 7). The energy of each system part can be divided by the mass of the LIB $m_{battery}$ and the SC m_{cap}. The sum of those two parts yields the specific energy E_{sp} of the PHESS (see Eq. 10).

$$E_{sp} = \frac{1}{m_{battery}} \int_0^\tau U_{battery}(t) i_{battery}(t) g(t)\, dt + \frac{1}{m_{cap}} \int_0^\tau U_{cap}(t) i_{cap}(t) g(t)\, dt \qquad (10)$$

To calculate the specific power P_{sp} of the PHESS, E_{sp} is divided by the product of the total test time τ and the factor D, which presents the fraction of time in which the current pulse is active during the test (see Eq. 11).

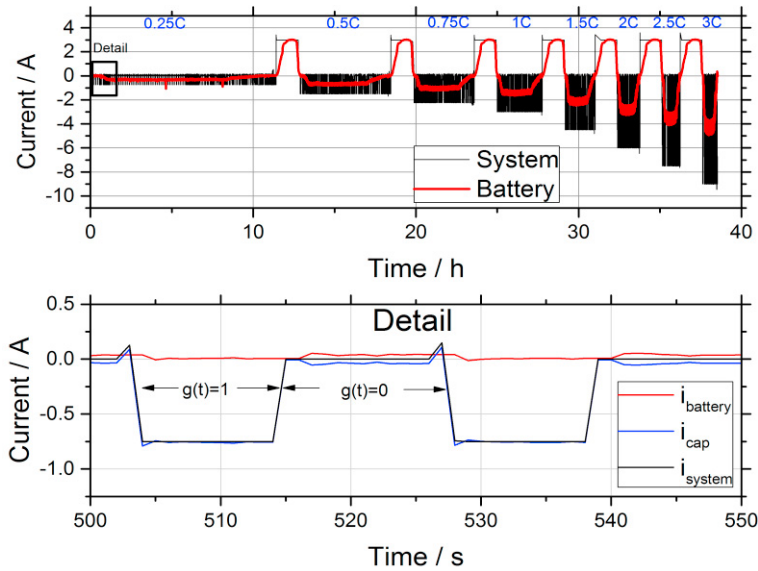$$P_{sp} = \frac{E_{sp}}{\tau D} \qquad (11)$$

Fig. 7. Measured currents of a PHESS LFP$_{LIC}$ during the test protocol (top). Detailed representation of the discharge pulse including the definition of factor g(t) (bottom).

4.3. Simulation setup: 48 V hybrid electric vehicle

Besides the experimental investigations of the power and energy density characteristics of different PHESS, we also show how PHESS perform in real applications and contrast them to ESS consisting of LIBs only. Therefore, we simulate a 48 V hybrid electric vehicle load profile and compare the charge throughput (Q in Ah) of a single LIB in the PHESS to those of a single LIB in the ESS. The charge throughput of the SC is not considered to be a performance criteria because of the high cycle lifetime of those technologies (>10,000 cycles). As the current running through serial connected cells is the same, we consider only the number of parallel connected cells to calculate Q per cell. We define the charge throughput ratio q_{PHESS}, which describes the percental difference between the charge throughputs of a LIB within an ESS and a PHESS. It is defined in Eq. 12 as follows:

$$q_{\text{PHESS}} = \left(\frac{Q_{\text{ESS}}}{p_{\text{ESS,battery}}} - \frac{Q_{\text{PHESS}}}{p_{\text{PHESS,battery}}} \right) \frac{Q_{\text{ESS}}}{p_{\text{ESS,battery}}}^{-1} 100\% \tag{12}$$

If q_{PHESS} has a positive value, the LIB in the ESS gets more strained than in the PHESS. If q_{PHESS} takes a negative value, it is the other way around.

For our data input we use the Worldwide harmonized Light vehicles Test Procedure (WLTP), which is used since September 2017 in the European Union to determine CO_2 emission and fuel consumption for passenger cars. Since the WLTP is only available as velocity (v) and acceleration (a) profile (see Fig. 9 (a)), we have to determine a current load profile to simulate the performance of our hybrid electric vehicle. We assume in our simulation a passenger car with a mass m_{car} of 1615 kg (e.g. AUDI A3 Sportback e-tron). With Eq. 13 we can calculate the power P_{car}, which is applied during operation. Additional physical effects, like rolling resistances, are not considered in this first approach.

$$P_{car} = m_{car} v a \tag{13}$$

In hybrid electric vehicles P_{car} is provided by a combustion engine (P_{CE}) and an electric drive train supplied by an ESS (P_{ESS}). A load management controls to what extent the combustion engine is supported by the electric drive train. Since we have no experimental data for P_{ESS} for a 48 V ESS under WLTP conditions, we assume in first-order the load management strategy represented in Fig. 8. If v of the car is below 50 kmh^{-1}, P_{car} will be supplied completely from the ESS (see Fig. 8 (a)). Between 50 kmh^{-1} and 70 kmh^{-1}, we assume a linear decrease of P_{ESS} from the applied power at 50 kmh^{-1} until 0 kW reached at 70 kmh^{-1} (see Fig. 8 (b)). Above a velocity of 70 kmh^{-1} the passenger car will be only powered by the combustion engine (see Fig. 8 (c)). In the case of slowdown, the ESS is charged by braking energy (see Fig. 8 (d)).
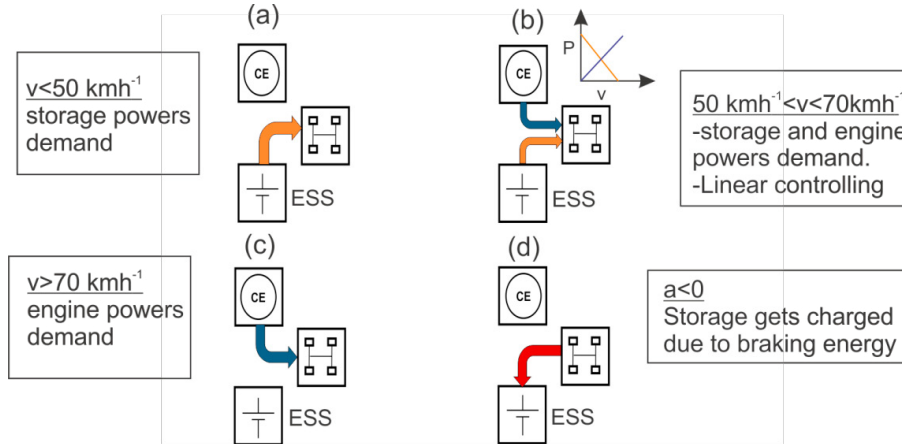

Fig. 8. Schematic representation of the assumed load management strategy for 48 V hybrid electric vehicles.

For the ESS we assume further constraints like a maximum power of 15 kW and a system voltage of 48 V, which are typical for commercial products in this segment on the market: With the system voltage of 48 V and P_{ESS} according to our load management strategy, the charge/discharge profile of the ESS I_{ESS} can be calculated. The load profiles represented as power or current profile are shown in Fig. 9 (b-c). A further constraint of this study is to not overstrain a single LIB ($i_{\text{battery}} \leq 3$ C). The system should also be able to power the application for a cumulative energy throughput of 3 kWh. The designed systems, which are subject of this study, are represented in Table 3. For a fair comparison we designed the PHESS to be similar in weight and volume to the equivalent ESS. The simulation starts at SOC of 50 % for the LIB bank.

Table 3. Overview of studied systems (including their weight and volume) for 48 V hybrid vehicle applications.

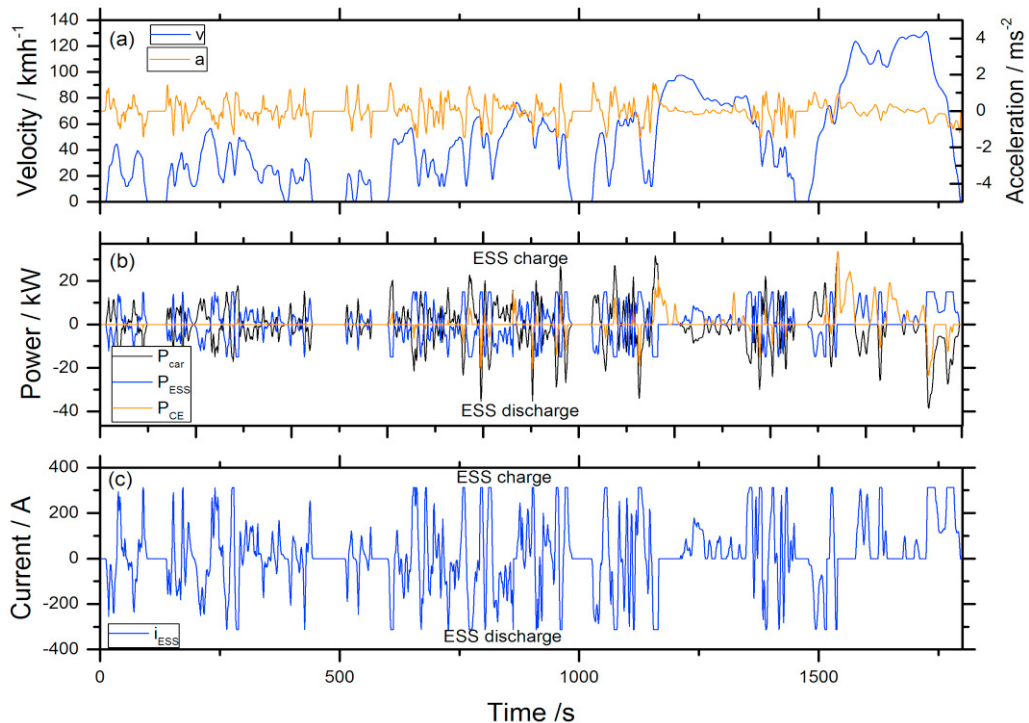| System	ESS LFP	PHESS LFP$_{LIC}$	PHESS LFP$_{UC}$	ESS LCO	PHESS LCO$_{LIC}$	PHESS LCO$_{UC}$
LIB	14S35P	14S30P	14S22P	12S42P	12S34P	12S25P
SC	-	14S1P	18S1P	-	13S1P	18S1P
Weight / kg	42	39	36	24	23	24
Volume / l	18	17	18	9	9	12

Fig. 9. Velocities and accelerations based on the WLTP procedure (top). Diagram of power flow within the power train, combustion engine and total power P_{car} (middle). Dynamic charge/discharge current profile of the ESS (bottom).

5. Results

5.1. Experimental results

The specific energy and specific power density of the analyzed systems is plotted in the Ragone diagram in Fig. 10. The individual systems are positioned in the expected areas. SCs show a high power but low energy density, while the LIBs show high energy density but low power density. We would expect a higher power density for the UC, but as mentioned before the maximum allowed current of the UC (approx. 1000 A) couldn't be realized based on the technical limits of the test channel.

The PHESS LFP$_{LIC}$ system achieves less energy density than the single LFP but therefore a double of power density, whereas the PHESS LFP$_{UC}$ shows less power and energy density than the PHESS LFP$_{LIC}$. More specifically, the energy density decreases from 84 Wh kg^{-1} to 60 Wh kg^{-1} and the power density from 186 W kg^{-1} to 146 W kg^{-1}. The PHESS LCO$_{LIC}$ system shows an extreme decrease of approx. 80 % in energy density compared to the LCO but has a small increase in power density from 140 to 180 W kg^{-1}. The PHESS LCO$_{UC}$ shows an energy density of 102 Wh kg^{-1} and a power density of 230 W kg^{-1}, which is an increase of 90 W kg^{-1} in power compared to the single LCO, however, with a decrease of energy density by around 45 %.
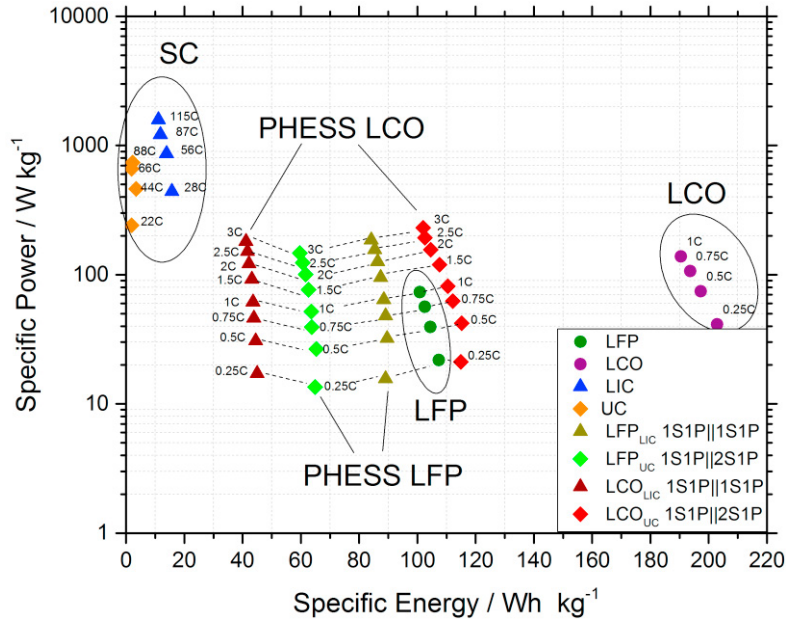
Fig. 10. Representation of the investigated specific energy and specific power of the studied PHESSs and single LIBs and SCs in a Ragone plot.

5.2. Simulation results

5.2.1. Validation

To validate the PHESS model we use the test protocol for the investigation of the power and energy density in Fig. 10. We compare the results of the model to the measurements for power and energy density values by using the root-mean-square error (RMSE) and the normalized root-mean-square error (NRMSE). Herein the result of the RMSE is normalized to the arithmetic mean value of the measurements for power and energy density for each system (see Eq. 14). The results for all PHESSs can be seen in Table 4.

$$x_m = \text{measurement value}$$
$$x_s = \text{simulaion value}$$
$$n = \text{number of data points}$$

$$RMSE = \sqrt{\frac{\sum_{i=1}^{n}(x_{m,i} - x_{s,i})^2}{n}}$$

$$NRMSE = \frac{RMSE}{\bar{x}_m}$$

(14)

The simulation of the PHESS LFP$_{LIC}$ shows a very small error, whereas the PHESS LCO$_{LIC}$ simulation shows deviation of approx. 10 % for the power density. Considering the NRMSEs of the PHESS LIB$_{UC}$, the maximum error is 9.2 % for the energy density of the PHESS LFP$_{UC}$. To the best of our knowledge no competitive NRMSE are given in the literature and we assume that the model is sufficiently accurate.

Table 4. Error calculation for the studied PHESSs for the calculation of the energy and power density.

	PHESS LFP$_{LIC}$	PHESS LCO$_{LIC}$	PHESS LFP$_{UC}$	PHESS LCO$_{UC}$
RMSE Energy density / Wh kg^{-1}	0.2	2.7	5.8	5.4
RMSE power density / W kg^{-1}	19.5	9.8	2.2	6.2
NRMSE energy density / %	2.9	6.2	9.2	5.0
NRMSE power density / %	2.1	10.2	3.0	5.5

5.2.2. 48 V hybrid electric vehicle study

The objective of this study is to analyze the load of a LIB within ESS vs. within several PHESSs. Fig. 11 shows the charge throughput ratio q_{PHESS} for an emulated 48 V hybrid electric vehicle for four PHESSs under the WLTP protocol. In general, we can see that the PHESSs are able to reduce the charge throughput of a single LIB compared to a LIB in a commercial ESS. Differences arise in the system setup for the PHESSs. The best result is achieved by the PHESS LCO$_{LIC}$ which reduces the charge throughput of its LIB by approx. 30 % compared to a LIB within the ESS LCO. In the PHESS LFP$_{LIC}$ we can see a reduction of the LIB load by 20 % in comparison to the LIB load within the ESS LFP. A reduction of approx. $15 - 19$ % is achieved for both PHESS LIB$_{UC}$. Notable is that the highest system dynamics arise at the beginning of the operations. Within PHESS$_{LIC}$ q_{HESS} achieves values of 40 and up to 50 % in charge throughput ratio, whereas PHESS$_{UC}$ shows reduced and even negative values, although they increase during the operation and result in positive values.
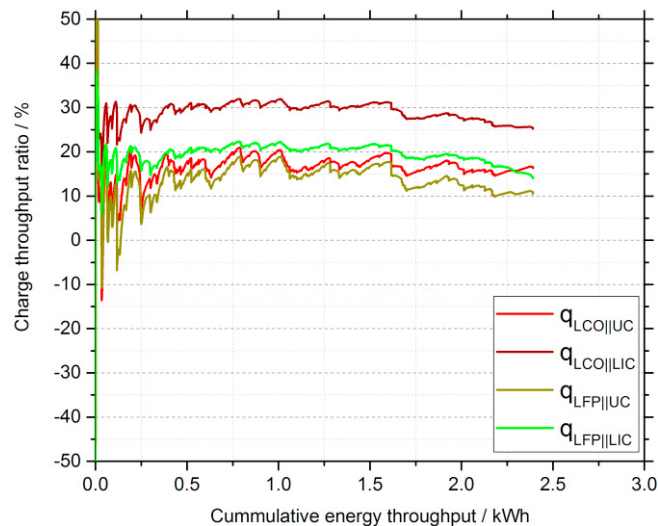
Fig. 11. Simulated comparison of the charge throughput ratio q$_{PH}$ for the PHESS listed in Table 3 using the WLTP profile.

6. Discussion

Our investigations show that the hybridization of LIBs and SCs through a passive parallel connection has certain advantages compared to systems, which are solely based on either SCs or LIBs.

In the experimental approach (see Fig. 10), the passive hybridization of a LCO with a UC achieves the best results. This system has s approx. 50 % smaller energy density than the single LCO, but approx. 26 % higher power density. Nevertheless, the LCO$_{UC}$ represents the highest energy density of all PHESSs under study. In the PHESS LCO$_{LIC}$ we can see that only 40 % of the capacity of the LCO can be used. The maximum allowed voltage is 3.8 V based on the upper voltage level of the LIC, which leads to a maximum SOC of 40 % of the LCO cell. As a

consequence the PHESS LCO$_{LIC}$ also does not show the expected advantages in comparison to its sole LCO.

In the PHESS LFP$_{LIC}$ system approx. 80 % of the capacity of the LFP cell can be used, which leads to a slightly reduced energy density compared to a single LFP. Also a double in power density can be achieved by the hybrid compared to a sole LFP. In contrast, a parallel connection of LFP with UC technology results in a further reduction of approx. 20 Wh kg^{-1} in energy density compared to the hybridization with LIC whilst reducing the power density at the same time. The reason is a twofold serial connected UC, which is necessary to match the voltage range of a LFP. Using two UCs the weight is increased which influences the power and energy density, whereas only one LIC is necessary to match the voltage range of the battery. Two UCs are also necessary to match the voltage range of a LCO but in comparison to the PHESS LCO$_{LIC}$ system, the LCO in the PHESS LCO$_{UC}$ defines the upper and lower cut-off voltage, which leads to a full utilization of the LCO capacity.

Regarding the results of our application-oriented simulation of 48 V system topologies, passive hybrid system can reduce the load of the LIB by 10 to 30 % in comparison to battery system of the same dimensions (in weight and volume). Herein the PHESS LCO$_{LIC}$ shows the maximum reduction by 30 %, whereas all the other PHESSs achieve similar reductions with 10 to 20 %. This reduction can lead to an increased lifetime of the entire energy storage system.

7. Conclusion

Subject of the experimental and model-based investigation has been the direct parallel connection of two types of lithium ion batteries with two types of supercapacitor technologies and the comparison of those passive hybrid systems to sole lithium ion battery systems within an application-oriented study, namely a 48 V hybrid electric vehicle energy storage system.

We have shown that the energy and power density of a passive hybrid system strongly depend on the matching of the voltage levels of the different technologies. A good fit results in maximum utilization of the lithium ion battery voltage range. Lithium iron phosphate cells match best with lithium ion capacitors, which lead to increased power density whilst remaining high energy density. In comparison a passive hybrid system made of lithium ion cobalt oxide and ultracapacitors results in an increase of 22 % in power density, but also a reduction of energy density compared to the sole LIB due to the additional weight of a second ultracapacitor. In application-oriented system designs, passive hybrid systems can reduce the load of the lithium ion battery by approx. 15 – 30 % in comparison to pure battery systems of the similar weight and volume. This result can be also interpreted as follows. A passive hybrid storage system can achieve approx. the same lifetime as a sole LIB system while weight and volume are reduced. The possible reduction in weight and volume and the associated cost reduction shall be part of further studies.

Acknowledgements

References

[1] G. Ning, B. Haran, and B. N. Popov, "Capacity fade study of lithium-ion batteries cycled at high discharge rates," *J. Power Sources*, vol. 117, no. 1–2, pp. 160–169, 2003.

[2] K. Naoi, S. Ishimoto, J. Miyamoto, and W. Naoi, "Second generation 'nanohybrid supercapacitor': Evolution of capacitive energy storage devices," *Energy Environ. Sci.*, vol. 5, no. 11, p. 9363, 2012.

[3] J. Ronsmans and B. Lalande, "Combining energy with power: Lithium-Ion Capacitors," *2016 Int. Symp. Power Electron. Electr. Drives, Autom. Motion, SPEEDAM 2016*, pp. 261–264, 2016.

[4] D. Cericola, P. Novák, A. Wokaun, and R. Kötz, "Hybridization of electrochemical capacitors and rechargeable batteries: An experimental analysis of the different possible approaches utilizing activated carbon, Li4Ti5O12 and LiMn2O 4," *J. Power Sources*, vol. 196, no. 23, pp. 10305–10313, 2011.

[5] A. Kuperman and I. Aharon, "Battery-ultracapacitor hybrids for pulsed current loads: A review," *Renew. Sustain. Energy Rev.*, vol. 15, no. 2, pp. 981–992, 2011.

[6] S. Y. Kan, M. Verwaal, and H. Broekhuizen, "The use of battery-capacitor combinations in photovoltaic powered products," *J. Power Sources*, vol. 162, no. 2 SPEC. ISS., pp. 971–974, 2006.

[7] C. Xiang, Y. Wang, S. Hu, and W. Wang, "A new topology and control strategy for a hybrid battery-ultracapacitor energy storage system," *Energies*, vol. 7, no. 5, pp. 2874–2896, 2014.

[8] S. K. Kollimalla *et al.*, "Multi-objective optimization of a semi-active battery/supercapacitor energy storage system for electric vehicles," *Appl. Energy*, vol. 135, no. 4, pp. 2–10, 2014.

[9] L. Gao *et al.*, "Power Enhancement of an Actively Controlled Battery / Ultracapacitor Hybrid Power Enhancement of an Actively Controlled Battery / Ultracapacitor Hybrid," vol. 20, no. 1, pp. 236–243, 2005.

[10] Y. Chuan, C. Mi, and M. Zhang, "Comparative study of a passive hybrid energy storage system using lithium ion battery and ultracapacitor," *World Electr. Veh. J.*, vol. 5, no. 1, pp. 83–90, 2012.

[11] D. Cericola, P. W. Ruch, R. Kötz, P. Novák, and a. Wokaun, "Simulation of a supercapacitor/Li-ion battery hybrid for pulsed applications," *J. Power Sources*, vol. 195, no. 9, pp. 2731–2736, 2010.

[12] H. He, R. Xiong, and J. Fan, "Evaluation of lithium-ion battery equivalent circuit models for state of charge estimation by an experimental approach," *Energies*, vol. 4, no. 4, pp. 582–598, 2011.

[13] A. Cordoba-Arenas, S. Onori, and G. Rizzoni, "A control-oriented lithium-ion battery pack model for plug-in hybrid electric vehicle cycle-life studies and system design with consideration of health management," *J. Power Sources*, vol. 279, no. 2015, pp. 791–808, 2015.

[14] L. Gao, S. Liu, and R. a. Dougal, "Dynamic lithium-ion battery model for system simulation," *IEEE Trans. Components Packag. Technol.*, vol. 25, no. 3, pp. 495–505, 2002.

[15] T. Huria, M. Ceraolo, J. Gazzarri, and R. Jackey, "High fidelity electrical model with thermal dependence for characterization and simulation of high power lithium battery cells," *2012 IEEE Int. Electr. Veh. Conf. IEVC 2012*, pp. 1–8, 2012.

[16] T. Grün, K. Stella, and O. Wollersheim, "Impacts on load distribution and ageing in Lithium-ion home storage systems," *Energy Procedia*, vol. 135, pp. 236–248, 2017.

[17] R. a. Dougal, S. Liu, and R. E. White, "Power and life extension of battery-ultracapacitor hybrids," *IEEE Trans. Components Packag. Technol.*, vol. 25, no. 1, pp. 120–131, 2002.

[18] C. E. Holland, J. W. Weidner, R. a. Dougal, and R. E. White, "Experimental characterization of hybrid power systems under pulse current loads," *J. Power Sources*, vol. 109, no. 1, pp. 32–37, 2002.